

## Nonlinear dynamics of a solid-state laser with injection

M. K. Stephen Yeung\* and Steven H. Strogatz†

*Department of Theoretical and Applied Mechanics, Kimball Hall, Cornell University, Ithaca, New York 14853-1502*

(Received 5 May 1998)

We analyze the dynamics of a solid-state laser driven by an injected sinusoidal field. For this type of laser, the cavity round-trip time is much shorter than its fluorescence time, yielding a dimensionless ratio of time scales  $\sigma \ll 1$ . Analytical criteria are derived for the existence, stability, and bifurcations of phase-locked states. We find three distinct unlocking mechanisms. First, if the dimensionless detuning  $\Delta$  and injection strength  $k$  are small in the sense that  $k = O(\Delta) \ll \sigma^{1/2}$ , unlocking occurs by a saddle-node infinite-period bifurcation. This is the classic unlocking mechanism governed by the Adler equation: after unlocking occurs, the phases of the drive and the laser drift apart monotonically. The second mechanism occurs if the detuning and the drive strength are large:  $k = O(\Delta) \gg \sigma^{1/2}$ . In this regime, unlocking is caused instead by a supercritical Hopf bifurcation, leading first to phase trapping and only then to phase drift as the drive is decreased. The third and most interesting mechanism occurs in the distinguished intermediate regime  $k, \Delta = O(\sigma^{1/2})$ . Here the system exhibits complicated, but nonchaotic, behavior. Furthermore, as the drive decreases below the unlocking threshold, numerical simulations predict a self-similar sequence of bifurcations, the details of which are not yet understood. [S1063-651X(98)05510-X]

PACS number(s): 05.45.+b, 42.65.Sf, 42.60.Mi, 42.55.Rz

### I. INTRODUCTION

The Adler equation

$$\frac{d\Phi}{dt} = \Delta - k \sin \Phi \quad (1)$$

provides the simplest model of phase locking between a nonlinear oscillator and an external periodic drive. Here  $\Phi(t)$  is the phase difference between the oscillator and the drive,  $\Delta$  is the frequency detuning, and  $k$  is the coupling strength. This equation first arose in connection with the phase locking of microwave oscillators [1], and has since found application in many other settings, including the depinning of charge-density waves [2], the entrainment of biological oscillators [3,4], and the onset of resistance in superconducting Josephson junctions [5,6].

A system governed by the Adler equation can display only two types of long-term behavior [6]. If  $|\Delta/k| \leq 1$ , all solutions tend to a phase-locked state, where the response oscillator maintains a constant phase difference relative to the driver. On the other hand, if  $|\Delta/k| > 1$ , all solutions exhibit phase drift, where the phase difference grows monotonically, with one oscillator periodically overtaking the other.

The main limitation of the Adler equation is that it treats the response oscillator as a system with only one degree of freedom, namely, its phase. Possible variations in its amplitude (and any other degrees of freedom) are ignored. This approximation is reasonable in the limit of weak driving; in that case, the amplitude of the response oscillator typically equilibrates much more rapidly than its phase, and can there-

fore be treated as a constant in the subsequent analysis. But if the driving is not weak (in some appropriate dimensionless sense), the dynamics can become complicated. In this paper we revisit a classic problem—the mathematical analysis of a solid-state laser with external injection [7–11]—and explore it in regimes where amplitude effects become important and the Adler approximation breaks down.

Our work was inspired by recent theoretical and experimental studies of amplitude effects in two mutually coupled solid-state Nd:YAG lasers [12,13]. In those studies, the lasers were equally coupled and identical, except for a slight relative detuning of their frequencies from some common cavity mode. For coupling strengths well above or below the locking threshold, the lasers were found to exhibit the simple behavior expected from the Adler approximation. However, as the coupling approached the locking threshold from below, the lasers showed a series of amplitude instabilities, culminating in a period-doubling route to chaos. These instabilities could not be explained by the Adler approximation. Instead the authors proposed the following mechanism. Below the locking threshold, the lasers exhibit phase drift. If the time required for one full cycle of phase slip happens to be an integer multiple of the lasers' relaxation period, the resulting subharmonic resonance might account for the observed instabilities. For the highly symmetrical case where the two lasers are assumed to have identical intensities and gains, this argument was proven to be correct by reducing the governing equations to those for a single, periodically modulated laser, where the subharmonic resonance mechanism was already known to occur [14,15].

We wondered whether similar amplitude instabilities and chaos would occur in two coupled Nd:YAG lasers with *unidirectional* coupling (or equivalently, in a single Nd:YAG laser with external injection). On the one hand, the qualitative argument about subharmonic resonances should still work. On the other hand, the equally coupled case enjoys special symmetries that are not present in the unidirectional

\*Author to whom correspondence should be addressed. Electronic address: yeung@tam.cornell.edu

†Electronic address: strogatz@cornell.edu

case. Given the crucial role of the symmetry in the earlier analyses of Erneux, Kuske, and Carr [12] and Thornburg *et al.* [13], it seemed possible that some new effects might occur if the symmetry were broken.

As we will show below, the system with one-way coupling can indeed display some fascinating behavior near the unlocking threshold, but it differs from that seen in the equally coupled case. In particular, we do not see a period-doubling route to chaos, nor any evidence of chaos at all. Instead, in a certain distinguished regime of parameters, we find a self-similar cascade of periodic windows and bifurcations. To the best of our knowledge, this bifurcation scenario is novel.

It will be interesting to see whether this cascade can be detected experimentally for a laser in the appropriate parameter regime, as specified by our theory. It would also be gratifying to have a better theoretical understanding of the cascade itself.

This paper is organized as follows. The governing equations are given in Sec. II. In Sec. III, we reduce the number of parameters by nondimensionalizing the equations and exploiting certain symmetries. By choosing a frame that corotates with the phase of the driver, we reduce the system to three coupled autonomous ordinary differential equations: one for  $\Phi(t)$ , the phase difference between the laser and the drive, and one each for the dimensionless gain and amplitude of the response laser. Fixed points of this reduced system correspond to injection-locked states of the original system. Section IV dispenses with the limiting cases of zero coupling or zero detuning where the dynamics can be analyzed straightforwardly.

The analysis begins in earnest in Sec. V, where we derive criteria for the existence and stability of injection-locked states, and compare our criteria to those obtained in the usual Adler approximation. In Secs. VI and VII, we start to investigate what happens when locking is lost. We show perturbatively that for a broad range of parameters, the phase difference  $\Phi(t)$  oscillates periodically, but the precise nature of those oscillations depends on the relative sizes of the dimensionless coupling, detuning, and stiffness of the system.

For a distinguished limit of parameters, described in Sec. VIII, the reduced system has complicated dynamics and undergoes the self-similar cascade of periodic windows and bifurcations mentioned above. In Sec. IX, we consider the system in the singular limit of zero stiffness. Again, the cascade persists. Based on the distinctive helical structure of the periodic orbits, we propose a mathematical mechanism underlying the cascade. It apparently stems from a codimension-two bifurcation in which a supercritical Hopf bifurcation combines with a saddle-node infinite-period global bifurcation. We have no proof of this mechanism, but show that it correctly predicts the scaling laws found numerically in the bifurcation diagram. We conclude with a discussion of open questions.

## II. FORMULATION OF THE MODEL

For solid-state lasers, as well as other Class B lasers with negligible linewidth enhancement factors, such as CO<sub>2</sub> and ruby (NMR) lasers [8], the polarization relaxes rapidly compared to the electric field and the gain, and can therefore be

adiabatically eliminated. Following Ref. [16] with straightforward modifications, we can write the following equations for two lasers coupled through transverse overlap of their electric fields, assuming single-mode operation and neglecting spatial variations within the lasers:

$$\begin{aligned} \frac{dE_1}{dT^*} &= \tau_{c,1}^{-1}[(G_1 - \alpha_1)E_1 + \mu KE'_2] + i\omega_1 E_1 + \sqrt{\epsilon_1} \xi_1(T^*), \\ \frac{dG_1}{dT^*} &= \tau_{f,1}^{-1}(p_1 - G_1 - G_1|E_1|^2), \\ \frac{dE_2}{dT^*} &= \tau_{c,2}^{-1}[(G_2 - \alpha_2)E_2 + KE'_1] + i\omega_2 E_2 + \sqrt{\epsilon_2} \xi_2(T^*), \\ \frac{dG_2}{dT^*} &= \tau_{f,2}^{-1}(p_2 - G_2 - G_2|E_2|^2). \end{aligned} \quad (2)$$

Here  $T^*$  is time, and for  $j=1,2$ ,  $E_j$  is the complex electric field,  $G_j$  is the gain,  $\tau_{c,j}$  is the cavity round-trip time,  $\tau_{f,j}$  is the fluorescence time of the lasing ions,  $p_j$  is the pump coefficient,  $\alpha_j$  is the cavity loss coefficient,  $\omega_j$  is the detuning of the laser from some common cavity mode, and  $K$  is a complex coupling coefficient with  $KE'_j$  representing the degree of overlap of the two lasers, with possible attenuation and dispersion taken into account. The noise term  $\sqrt{\epsilon_j} \xi_j(T^*)$  models spontaneous emission, but for simplicity, we will consider only the noiseless case  $\epsilon_j=0$ . Also, we will assume the media are linear, nonabsorbing and nondispersive and the coupling is dissipative so that  $E'_j = E_j$  and  $K$  is real.

The parameter  $\mu$  in the first equation above is a symmetry-breaking coefficient measuring the extent of the feedback from the second laser to the first. The case of symmetric coupling ( $\mu=1$ ,  $\tau_{c,1}=\tau_{c,2}$ ,  $\tau_{f,1}=\tau_{f,2}$ ) has been analyzed in [13]. In this paper, we focus instead on the case of unidirectional coupling, i.e.,  $\mu=0$ . When  $\mu=0$ , the first laser is unaffected by the second, and hence we may regard it as a driver. Assuming that this driving laser is pumped above its lasing threshold ( $p_1 > \alpha_1$ ), it is easy to show that its amplitude and phase velocity settle down to constant values. Specifically, the long-term state of the drive is given by  $E_1 = \sqrt{p_1/\alpha_1 - 1} \exp[i(\Phi_{10} + \omega_1 T^*)]$ , where  $\Phi_{10}$  is an arbitrary constant, with constant gain  $G_1 = \alpha_1$ .

We assume these forms for  $E_1$  and  $G_1$  in the rest of the analysis. Thus, although we have formulated our study in terms of one solid-state laser driving another, the arguments and results we present hold for more general situations, such as a solid-state laser subjected to optical injection by other sources.

In a typical experimental setup using Nd:YAG lasers [13],  $\tau_{f,j}$  and  $\tau_{c,j}$  are both positive and are of the orders  $10^{-4}$  s and  $10^{-10}$  s, respectively. Thus we have two vastly different time scales in the system. The detuning  $\omega_1 - \omega_2$  and the coupling  $K$  are control parameters. The detuning has values typically of order  $10^5$  Hz, while the coupling can be varied over several orders of magnitude. In the symmetrically coupled system [13], values of  $K$  ranging from  $O(10^{-8})$  to  $O(10^{-2})$  have been used. The pump  $p_j$  and the loss  $\alpha_j$  are both positive,  $O(10^{-2})$  and their ratio  $p_j/\alpha_j$  is typically an  $O(1)$  quantity.

### III. SCALING AND SYMMETRIES

We scale the equations governing the response laser by introducing the following dimensionless quantities:

$$\sigma = \frac{\tau_{c,2}}{\alpha_2 \tau_{f,2}}, \quad B = \frac{p_2}{\alpha_2}, \quad \tau = \frac{\alpha_2 T^*}{\tau_{c,2}}, \quad F_2 = \frac{G_2}{\alpha_2}.$$

Here  $\sigma$  is a stiffness parameter, typically  $O(10^{-4})$  in experiments, characterizing the vast difference in the time scales of the cavity round trip and fluorescence times in the response laser. The smallness of  $\sigma$  will be important in the subsequent analysis. The parameter  $B$  is the dimensionless pump strength of the response laser; it often plays the role of a control parameter in what follows. The variables  $\tau$  and  $F_2$  represent dimensionless time and gain, respectively.

Next we change variables by going into a reference frame rotating with the driver. Let  $X_2 \geq 0$  be the amplitude of the complex field  $E_2$ , defined by

$$E_2 = X_2 e^{i\Phi_2},$$

and define  $\Phi$  by  $\Phi = \Phi_2 - \Phi_1$ , where  $\Phi_1$  is the phase of the driving laser and  $\Phi \sim \Phi_2 - \Phi_{10} - (\omega_1 \tau_{c,2} / \alpha_2) \tau$  for sufficiently large  $\tau$ . Assuming [17]  $X_2 \neq 0$ , we obtain the reduced system

$$\frac{dX_2}{d\tau} = (F_2 - 1)X_2 + k \cos \Phi, \quad (3a)$$

$$\frac{d\Phi}{d\tau} = \Delta - \frac{k}{X_2} \sin \Phi, \quad (3b)$$

$$\frac{dF_2}{d\tau} = \sigma(B - F_2 - F_2 X_2^2), \quad (3c)$$

where

$$\Delta = \frac{(\omega_2 - \omega_1) \tau_{c,2}}{\alpha_2}, \quad k = \frac{K \sqrt{p_1 / \alpha_1 - 1}}{\alpha_2}. \quad (4)$$

Here,  $\Delta$  is a dimensionless measure of the frequency detuning of the two lasers, and  $k$  can be interpreted as either a dimensionless coupling strength or injection amplitude.

By choosing the phase difference  $\Phi$  as a variable, we have eliminated the explicit time dependence in the original system by rotating with the phase of the driver. In this rotating reference frame, a steady state now means a state in which the phase difference between the two lasers, and not the phase  $\Phi_2$  of the second laser itself, is constant. Such a state is said to be phase locked. The particular case in which  $\Phi = 0$  (which is possible if and only if  $\Delta = 0$ ) is called the coherent or in-phase state.

The analysis of the reduced system (3) will occupy most of this paper. As Eq. (3) is invariant under

$$\Delta \rightarrow -\Delta, \quad \Phi \rightarrow -\Phi, \quad (5)$$

as well as under

$$k \rightarrow -k, \quad \Phi \rightarrow \pi + \Phi, \quad (6)$$

we will assume from now on that  $k, \Delta \geq 0$ . Also,  $\sigma, B \geq 0$  by definition.

There is a slight catch that one should be aware of. Although we can assume  $k \geq 0$  without any loss of mathematical generality, there can still be physical consequences. For example, the symmetry (6) allows us to change the sign of  $k$ , but at the cost of transforming an in-phase solution to an antiphase one. In fact, for certain systems of coupled lasers,  $k$  can be negative [16].

### IV. SPECIAL CASES

The special case  $k = 0$  with general  $\Delta$  is trivial: the driver and the response laser are decoupled. The reduced system (3) has a global attractor that is typically a periodic orbit, corresponding to phase drift between the laser and the drive. In degenerate cases, the attractor can be a fixed point for Eq. (3), e.g., if there is also no detuning, or if the pump for the response laser lies below the lasing threshold.

A more important special case is that of zero detuning:  $\Delta = 0$  with  $k \neq 0$ . Then  $\Phi = 0$  (in-phase) and  $\Phi = \pi$  (antiphase) are invariant manifolds [18], the former attracting all initial conditions except those on the latter, which is repelling. Hence, so far as long-time behaviors are concerned, we can confine our attention to the flow restricted to the manifold  $\Phi = 0$ .

On  $\Phi = 0$ , Eq. (3) simplifies to the planar vector field

$$\frac{dX_2}{d\tau} = (F_2 - 1)X_2 + k, \quad (7)$$

$$\frac{dF_2}{d\tau} = \sigma(B - F_2 - F_2 X_2^2).$$

The nullclines [6] are

$$F_2 = 1 - \frac{k}{X_2}, \quad (8a)$$

$$F_2 = \frac{B}{1 + X_2^2}. \quad (8b)$$

Since Eq. (8a) represents an increasing function of  $X_2$  while Eq. (8b) represents a decreasing one, there can be at most one real intersection. On the other hand, we may combine the two equations into a cubic polynomial equation in  $F_2$ :

$$F_2[(F_2 - 1)^2 + k^2] - B(F_2 - 1)^2 = 0$$

and see that there is at least one real solution in the interval  $(0, \min(1, B))$ , by the intermediate value theorem. Hence there is precisely one solution for  $F_2$  in  $(0, \min(1, B))$ , corresponding to a unique fixed point. An application of Dulac's criterion and the Poincaré-Bendixson theorem [6] to Eq. (7) then reveals that this fixed point is actually globally stable with respect to perturbations on the  $X_2 F_2$  plane. Hence, in physical terms, a globally stable in-phase state exists if and only if there is no relative detuning between the two lasers.

Having exhausted the possibilities for these special cases, we will assume  $k, \Delta \neq 0$  from now on.

## V. LOCKED STATES

### A. Existence and stability for general parameter values

A locked state of the laser system corresponds to a fixed point of Eq. (3), which must satisfy

$$\begin{aligned} (F_2 - 1)X_2 + k \cos \Phi &= 0, \\ \Delta - \frac{k}{X_2} \sin \Phi &= 0, \\ B - F_2 - F_2 X_2^2 &= 0. \end{aligned} \quad (9)$$

In the limiting case  $B=0$  (i.e., the response laser is not pumped) Eq. (9) can be readily solved to yield

$$F_2 = 0, \quad X_2 = \frac{k}{\sqrt{1 + \Delta^2}}, \quad \Phi = \tan^{-1} \Delta.$$

The eigenvalues of the Jacobian at this fixed point are

$$\lambda_1 = -\sigma \left( 1 + \frac{k^2}{1 + \Delta^2} \right), \quad \lambda_2, \lambda_3 = -1 \pm i\Delta,$$

all having negative real parts. This means, as  $\Phi$  is the phase difference between the two lasers, that the response laser is passively driven into stable periodic motion

$$E_2 = \frac{k}{\sqrt{1 + \Delta^2}} \exp \left[ i \left( \tan^{-1} \Delta + \Phi_{10} + \frac{\omega_1 \tau_{c,2}}{\alpha_2} \tau \right) \right]$$

with a constant phase-lead  $\tan^{-1} \Delta$  ahead of the driver, even though it is not pumped.

For  $B > 0$  so that  $F_2 \neq 0$  at a fixed point, we may eliminate  $\Phi$  from Eq. (9) and get

$$X_2^2 = \frac{B}{F_2} - 1, \quad (10a)$$

$$X_2^2 = \frac{k^2}{(F_2 - 1)^2 + \Delta^2}. \quad (10b)$$

Consider the graphs of  $X_2$  versus  $F_2$  corresponding to Eqs. (10a,10b). The intermediate value theorem reveals the following. (i) If  $0 < B \leq 1$ , there is only one fixed point, with  $F_2 \in (0, B) \subseteq (0, 1)$ . (ii) If  $1 < B < B_c$ , depending on parameter values, there may be one or three fixed points. There is always one in the interval  $F_2 \in (0, 1)$ , and there may be a pair in  $F_2 \in (1, B)$ . (iii) If  $B > B_c$ , again depending on parameter values, there may be one or three fixed points, all of which lie in  $F_2 \in (1, B)$ . Here

$$B_c \equiv 1 + \frac{k^2}{\Delta^2} \quad (11)$$

represents a special value for the dimensionless pump strength. In Sec. VB we will show that  $B_c$ , with a small correction, is the critical value at which locked states lose stability.

To analyze the local stabilities of these fixed points, we apply the Routh-Hurwitz criteria [19,20] to the characteristic equation of Eq. (3), and deduce that the fixed point is locally stable if and only if

$$\begin{aligned} H_1(F_2) &:= (B + 2)F_2^2 - 2F_2^3 - B(1 + \Delta^2) < 0, \\ H_2(F_2) &:= 2\sigma(F_2^2 - B) - F_2[(F_2 - 1)^2 + \Delta^2] < 0, \\ H_2'(F_2) &:= 2F_2(F_2 - 1) - \sigma B < 0, \\ H_3(F_2) &:= 2(F_2 - 1)^3 + 2\Delta^2(F_2 - 1) - \frac{2\sigma B}{F_2}(F_2 - 1)(F_2 - 2) \\ &\quad - 2\sigma F_2(F_2 - 1) + 2\sigma^2 B - \frac{2\sigma^2 B^2}{F_2^2} < 0, \end{aligned} \quad (12)$$

where  $F_2$  is evaluated at the fixed point in question. When  $H_1, H_3 < 0$ , the two inequalities  $H_2 < 0$  and  $H_2' < 0$  are equivalent and so we only need to check one of them.

For  $B < B_c$ , we can verify by direct substitution into condition (12) that the fixed point with  $F_2 < 1$  is stable. As we increase  $B$  through  $B_c$ , this fixed point crosses  $F_2 = 1$ . The stabilities for the fixed points with  $F_2 > 1$  are not so clear. In fact, at  $B = B_c$  we can solve the fixed-point equation (10) exactly and find that either  $F_2 = 1$  or

$$F_2 = 1 + \frac{k^2}{2\Delta^2} \pm \sqrt{\frac{k^4}{4\Delta^4} - \Delta^2 - k^2},$$

where the last pair exist if and only if  $k^4/4\Delta^4 \geq \Delta^2 + k^2$ . Direct substitution into condition (12) reveals that the fixed point with  $F_2 = 1$  is stable (while the stabilities of the other two fixed points remain unclear) and hence there is no bifurcation at  $B = B_c$ . Hence, the condition  $B < B_c$  is sufficient but not necessary for a stable locked state to exist. In fact, for  $\sigma = O(1)$ , we have found numerical examples of stable locked states even when  $B > B_c$ . However, these examples are not of much physical interest, given that  $\sigma \ll 1$  for real lasers. In the next subsection, we will show that for  $\sigma \ll 1$ , the locking condition  $B < B_c$  is indeed tight, with a correction term that approaches zero as  $\sigma$  does.

### B. Location and stability of locked states for $\sigma \ll 1$

From now on we will assume  $\sigma \ll 1$ . For definiteness, consider the scaling  $k, \Delta = O(\sigma^a)$ , and write

$$k = \kappa \sigma^a, \quad \Delta = \delta \sigma^a.$$

For  $a > 0$ , the graph of Eq. (10b) has a narrow peak, with  $O(\sigma^a)$  width, at  $F_2 = 1$ , and we can show that there are three fixed points of Eq. (3) if  $B \leq B_c$ , while there is only one fixed point if  $B > B_c$  and  $B - B_c \gg \sigma^{2a}$ . As we increase  $B$ , somewhere in the region  $B_c < B \leq B_c + O(\sigma^{2a})$ , two of the fixed points collide. To better understand what is going on, we will employ the Routh-Hurwitz criteria (12).

For  $B > 1$ , we can find the location of the fixed points perturbatively if  $a > 0$ . There is always a fixed point with

$$F_2 = F_0^* \equiv B - \frac{\sigma^{2a} \kappa^2 B}{(B - 1)^2} + O(\sigma^{4a}). \quad (13)$$

For  $1 < B \leq B_c$ , there are a pair of fixed points [21] with

$$F_2 = F_{\pm}^* \equiv 1 \pm \sigma^a \sqrt{\frac{\kappa^2}{(B-1)} - \delta^2} + O(\sigma^{2a}). \quad (14)$$

Direct substitution into Eq. (12) shows that only the fixed point with  $F_2 = F_-^*$  is stable. So we will concentrate on this fixed point and study the mechanism through which it loses stability. We expect that it will undergo a bifurcation in  $B_c < B \leq B_c + O(\sigma^{2a})$ .

Bifurcation occurs if one of the functions in Eq. (12) vanishes [22]. Specifically, the Routh-Hurwitz condition  $H_1 = 0$  corresponds to a zero eigenvalue, and is therefore generically associated with a saddle-node bifurcation, whereas  $H_3 = 0$  indicates pure imaginary eigenvalues and a Hopf bifurcation. (These results follow immediately from the observation that the characteristic polynomial is cubic with real coefficients.)

We solve Eq. (12) in conjunction with the fixed-point equation (10) by the method of dominant balance [23]. Let  $B = B_c + \varepsilon$ . Then  $H_1(F_2) = 0$  if

$$\varepsilon = \varepsilon_1 \equiv \frac{\sigma^{2a} \delta^2 B_c^2}{4(B_c - 1)} + O(\sigma^{4a}), \quad (15)$$

$$F_2 = 1 + \frac{\sigma^{2a} \delta^2 B_c}{2(B_c - 1)} + O(\sigma^{4a}),$$

and  $H_3(F_2) = 0$  if

$$\varepsilon = \varepsilon_3 \equiv \sigma^{2-2a} B_c^2 (B_c - 1) / \delta^2 + O(\sigma^{3-4a}), \quad (16)$$

$$F_2 = 1 + \sigma^{2-2a} B_c (B_c - 1) / \delta^2 + O(\sigma^{3-4a}) \quad \text{for } a < 1/2.$$

There is no self-consistent solution, with  $0 < \varepsilon \ll 1$ , for  $H_3(F_2) = 0$  if  $a > 1/2$ . If  $a < 1/2$ , then  $\varepsilon_3 \ll \varepsilon_1$  and so  $H_3$  becomes zero before  $H_1$  does, indicating a Hopf bifurcation. (Whether it is subcritical or supercritical is undetermined at this stage in the calculation. But see Sec. VII B.) If  $a > 1/2$ , then  $H_1$  becomes zero at  $\varepsilon = \varepsilon_1$ , indicating a zero-eigenvalue bifurcation, which, given the absence of any appropriate symmetry, is expected to be a saddle-node bifurcation [18]. We have confirmed these bifurcation scenarios numerically, using the bifurcation package AUTO [24].

The argument above leaves a gap at  $a = 1/2$ , in which case  $H_1$  and  $H_3$  both vanish when  $\varepsilon = O(\sigma)$ , corresponding to a bifurcation of higher codimension, and potentially leading to a complicated outcome. We will look into this case separately in Sec. VIII. But as far as the fixed point is concerned, it loses stability at  $B = B_c + O(\sigma)$ . Hence, no matter whether the scaling exponent  $a$  is greater than, less than, or equal to  $1/2$ , we can conclude that  $B_c$  is a tight estimate of the unlocking threshold, with an error at most of  $O(\sigma)$ .

To sum up, for  $\sigma \ll 1$  we have shown the following: (i) If  $B < B_c + \varepsilon$ , there is one locally stable fixed point. This corresponds to a stable injection-locked state, with a nonzero phase difference unless there is no detuning. (ii) If  $B > B_c + \varepsilon$ , then there may be one or three fixed points, all in the region  $F_2 \in (1, B)$ , and they are all saddles. Hence there is no stable locked state in this case. Here,  $0 < \varepsilon = \min(\varepsilon_1, \varepsilon_3)$

$\leq O(\sigma)$ , with  $\varepsilon_1, \varepsilon_3$  given by Eqs. (15) and (16), and  $B = B_c + \varepsilon$  is the parameter value at which the unlocking transition occurs.

Taking advantage of the symmetries (5) and (6), we may rewrite the locking condition  $B < B_c + \varepsilon$  in terms of the physical parameters defined in Eq. (2):

$$|K| \sqrt{\frac{p_1}{\alpha_1} - 1} > |\omega_1 - \omega_2| \tau_{c,2} \sqrt{\frac{p_2}{\alpha_2} - 1} - \varepsilon, \quad (17)$$

with  $0 < \varepsilon \leq O(\tau_{c,2}/\alpha_2 \tau_{f,2})$ . In physical terms, stable locking occurs if the coupling  $K$  and the injection intensity (controlled by the pump strength  $p_1$ ) are sufficiently strong to overcome the relative detuning between the drive and the response laser.

It is also noteworthy that the right-hand side of the locking condition depends on the pump strength  $p_2$  of the response laser. In applications involving injection locking, a laser with a low power output but very accurate frequency is often used to control a strong but sloppy one. The criterion (17) indicates that locking is more difficult if the response laser has a stronger pump  $p_2$ .

### C. Discussion

The condition for locking is commonly derived in the limit of small injection intensity (which equals  $p_1/\alpha_1 - 1$  in our notation). This derivation relies on the slowly varying envelope approximation, along with the further assumptions that the intensity of the response laser is at the free-running output level and that the gain has saturated. Then the system of governing equations is reduced to a phase model equivalent to Adler's equation [7,11]. The traditional result for the locking condition is, in terms of our symbols,  $\Delta < k/\sqrt{I_2}$  where  $I_2$  is the free-running intensity of the driven laser. Since  $I_2 = B - 1$ , this condition reduces to our condition  $B < B_c$ .

We have rederived this well known result in a more general context. In particular, we have shown that a sufficient condition for locking is  $B < B_c$ , even when  $k$  is *not* small and the phase model no longer holds. [Recall that  $k$  is the dimensionless product of the coupling strength and the injection amplitude; see Eq. (4).] Moreover, our approach allows us to calculate the correction terms in the formulas for the locking threshold, namely, Eqs. (15) and (16), in the limit of small  $\sigma = \tau_{c,2}/(\alpha_2 \tau_{f,2})$ .

To see why a simple phase model can give the correct locking condition, consider the least-stable eigendirection of the locked state. Suppose the coupling is weak, in the sense that  $k = O(\Delta) \ll \sigma^{1/2}$ . At the bifurcation point, the soft mode (the eigenvector associated with the zero eigenvalue) is given by

$$(X_2, \Phi, F_2) = \left( -\sigma^a, \frac{2(B_c - 1)}{\kappa B_c}, \frac{2\sigma^a \kappa}{\delta B_c} \right) + O(\sigma^{2a}).$$

For small  $\sigma$ , the first and third components of this eigenvector are small, indicating that the soft mode lies nearly along the phase direction. Hence when the coupling is weak, the phase direction alone determines the locking condition, to a good approximation.

More generally, one can ask, When can the full model be replaced by a phase model? We will show in the following section that this reduction is valid when  $k$  and  $\Delta$  are small.

## VI. WEAK COUPLING

If  $B > B_c + \varepsilon$ , there is no stable fixed point of Eq. (3), so the response laser cannot lock to the drive. The desynchronized dynamics then strongly depend on the relative sizes of the parameters  $k$ ,  $\Delta$ , and  $\sigma$ . For definiteness we will continue to assume that  $\sigma \ll 1$  and  $k, \Delta = O(\sigma^a)$ .

In this section, we focus on the weak coupling case  $a > 1/2$ , and show that unlocking occurs via a saddle-node infinite-period bifurcation. All solutions are then attracted to a stable periodic solution for the reduced system; this periodic solution corresponds physically to a phase-drifting state.

Before we go on, a warning is in order: we will consider only lowest-order effects in this section for simplicity. In particular, we will not pick up the  $\varepsilon$  corrections [Eqs. (15) and (16)] for the locking condition.

Suppose that  $k = O(\Delta) \ll \sigma^{1/2}$ , or equivalently,

$$|K| \sqrt{\frac{p_1}{\alpha_1} - 1} \sim |\omega_1 - \omega_2| \tau_{c,2} \ll \sqrt{\frac{\alpha_2 \tau_{c,2}}{\tau_{f,2}}}$$

in terms of the physical parameters in Eq. (2). In this limit, we can reduce the full model Eq. (3) to a phase model by the following argument. Let  $u = F_2 - 1$  and introduce the self-consistent assumption  $X_2 = O(1)$  (which we find to be justified by numerics). Then we observe that if  $u \gg k$ , the term  $k \cos \Phi$  in Eq. (3a) is negligible and so the  $X_2, u$  dynamics decouples from that of  $\Phi$  and constitutes a two-dimensional system. Next, by a phase plane analysis and diagonalizing the Jacobian we can show that  $X_2 \rightarrow \sqrt{B-1}$  and  $u$  decreases toward 0, with an  $O(\sigma^{1/2})$  spiralling frequency and an  $O(\sigma)$  relaxation rate. So after an  $O(\sigma^{-1})$  transient time,  $u$  becomes comparable to  $k$  and we can no longer neglect the term  $k \cos \Phi$  in Eq. (3a).

As  $X_2 = O(1)$ , Eq. (3b) indicates that  $\Phi$  evolves with a characteristic rate of size  $O(\Delta, k)$ . If this characteristic rate is much smaller than that for the spiralling  $X_2, u$  dynamics, which is true if  $\Delta, k \ll \sigma^{1/2}$ , we can take  $k \cos \Phi$  to be a constant with an  $O(k^2)$  error, and deduce that  $X_2, u$  relax to their equilibrium values with an  $O(\sigma^{1/2})$  characteristic rate.

Assuming this relaxation has happened, Eq. (3b) becomes

$$\frac{d\Phi}{d\tau} = \Delta - \frac{k}{\sqrt{B-1}} \sin \Phi + O(k^2), \quad (18)$$

which is recognized as Adler's equation [Eq. (1)]. The important feature is that  $\Phi$  either approaches a constant or is strictly increasing, with  $\Phi \bmod 2\pi$  being periodic with period  $2\pi/\sqrt{\Delta^2 - k^2/(B-1)}$ , depending on whether  $B$  is smaller than or larger than  $1 + k^2/\Delta^2$ , with an  $O(k^2)$  error.

So, for large  $\tau$ , the unlocked dynamics are given by

$$X_2 \sim \sqrt{B-1} + \frac{kB \cos \Phi(\tau)}{2(B-1)} + O(k^2), \quad (19)$$

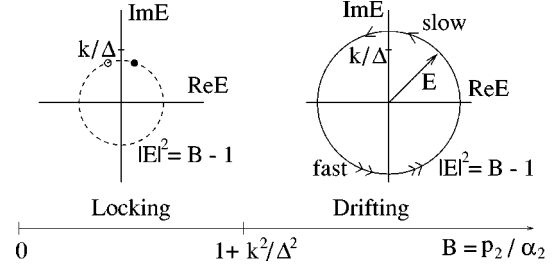


FIG. 1. The dependence of the behaviors of the phase difference  $\Phi$  on the pump to loss ratio  $B$ , for  $k \sim \Delta = O(\sigma^a)$ ,  $a > 1/2$ .  $\Delta, k$  are as defined in Eq. (4).  $E = X_2 e^{i\Phi}$  is the complex electric field. The stable (unstable) fixed point is represented by  $\bullet$  ( $\circ$ ).  $\Phi$  is constant if  $B < B_c \equiv 1 + k^2/\Delta^2$  and increases strictly if  $B > B_c$ , with a saddle-node infinite-period bifurcation at  $B = B_c$ . The bifurcation value for  $B$  has  $O(\sigma^{2a})$  errors [Eq. (15)] and the value of  $X_2$  has  $O(\sigma^a)$  errors [Eq. (19)]. Contrast this with Fig. 2.

$$F_2 \sim 1 - \frac{k \cos \Phi(\tau)}{\sqrt{B-1}} + O(k^2),$$

where  $\Phi(\tau)$  is governed by Eq. (18). Hence  $X_2(\tau)$  and  $F_2(\tau)$  oscillate periodically, with  $O(k)$  amplitudes and the same Fourier spectra as  $\cos \Phi$ , up to overall multiplicative constants. This last feature supplements the observation, noted in [7(a)], that the laser intensity ‘‘acquires distortion at higher harmonics’’ as the locking threshold is approached. In fact, by insisting on a phase model, Siegman [7(b)] analyzed the dynamics of a laser with external injection outside the locking regime. Now we have justified this insistence by showing that in an appropriate regime in the parameter space, namely,  $k = O(\Delta) \ll \sigma^{1/2}$ , the laser system indeed approaches a state with  $X_2 \approx \sqrt{B-1}$ ,  $F_2 \approx 1$ , starting from arbitrary initial conditions.

The saddle-node bifurcation found in Sec. VB for  $a > 1/2$  can now be identified more specifically as a saddle-node infinite-period bifurcation [6]. For  $B > B_c + \varepsilon$ , the phase increases strictly with a nonuniform speed, with a bottleneck near  $\Phi = \sin^{-1}(\Delta\sqrt{B-1}/k)$ . These behaviors are illustrated in Fig. 1.

The argument above clearly does not hold if  $k, \Delta = O(\sigma^{1/2})$ , as then the phase dynamics has a characteristic rate comparable to that of the spiralling motion on the  $uX_2$  cross sections. We will address this case in Sec. VIII.

## VII. STRONG COUPLING

We turn now to the case of strong coupling:  $k = O(\Delta) \gg \sigma^{1/2}$ . The main result is that unlocking occurs via a supercritical Hopf bifurcation, leading to a globally attracting limit cycle for Eq. (3) when  $B > B_c + \varepsilon$ . We will investigate in Sec. VII A the case  $k = O(\Delta) = O(1)$ . Then in Sec. VII C we use a rescaling argument to show that this scenario also subsumes the ostensibly more general case  $k = O(\Delta) \gg \sigma^{1/2}$ .

### A. Two-timing calculations

Assume that  $\sigma \ll 1$ , and  $k, \Delta = O(1)$ . By defining

$$E = X_2 e^{i\Phi},$$

which represents the complex electric field of the response laser as observed in a frame rotating with the driver, we can combine Eqs. (3a) and (3b) into

$$\frac{dE}{d\tau} = [(F_2 - 1) + i\Delta]E + k. \quad (20)$$

For  $\sigma \ll 1$ ,  $F_2$  is slowly varying and so may be taken to be a constant except over long-time scales of order  $O(1/\sigma)$ . If  $F_2$  were really a constant, the exact solution to Eq. (20) could be found as

$$E = E_c \exp[(F_2 - 1) + i\Delta]\tau - \frac{k}{(F_2 - 1) + i\Delta}, \quad (21)$$

where  $E_c$  is a complex constant. Hence  $X_2 = |E|$  would decay exponentially to  $k/\sqrt{(F_2 - 1)^2 + \Delta^2}$  if  $F_2 < 1$  and grow exponentially to infinity if  $F_2 > 1$ . In the first scenario where  $F_2 < 1$ , we have

$$\frac{dF_2}{d\tau} \approx \sigma \left[ B - F_2 \left( 1 + \frac{k^2}{(F_2 - 1)^2 + \Delta^2} \right) \right] > 0$$

if  $B > B_c$  and  $F_2 \approx 1$ . So  $F_2$  would grow for  $F_2 < 1$ . In the second case where  $F_2 > 1$ ,  $dF_2/d\tau \approx -\sigma F_2 X_2^2 < 0$  and so  $F_2$  would decay. Hence we expect that, after initial transient instabilities for  $\tau \ll O(1/\sigma)$ , the system will settle down to its eventual fate, with  $F_2 \approx 1$  and  $E \approx E_c \exp(i\Delta\tau) + ik/\Delta$  for all sufficiently large  $\tau$ , and this is indeed what we find in our numerics (not shown).

Now we investigate the structure of the attractor of Eq. (3) by two timing [23]. We first define a slow time  $T = \sigma\tau$ . Abusing notation, we have

$$\frac{d}{d\tau} f(\tau, T) = \frac{\partial f}{\partial \tau} + \sigma \frac{\partial f}{\partial T},$$

where  $f$  denotes either  $F_2$  or  $E$ . Assuming transients have already decayed, we let  $F_2 = 1 + \sigma F_2^{(1)} + O(\sigma^2)$  and  $E = E^{(0)} + \sigma E^{(1)} + O(\sigma^2)$ . Then we find

$$E^{(0)} = A^{(0)}(T) e^{i[\theta^{(0)}(T) + \Delta\tau]} + \frac{ik}{\Delta},$$

$$F_2^{(1)} = f(T) + \left( B - 1 - [A^{(0)}(T)]^2 - \frac{k^2}{\Delta^2} \right) \tau + \frac{2k}{\Delta^2} A^{(0)}(T) \times \cos(\theta^{(0)}(T) + \Delta\tau).$$

To remove the secularity so that  $F_2^{(1)}$  remains bounded (which is necessary for  $F_2$  to stay close to 1), we need

$$A^{(0)} = \sqrt{B - \left( 1 + \frac{k^2}{\Delta^2} \right)} = \sqrt{B - B_c}. \quad (22)$$

This is well defined if and only if  $B \geq B_c$ , which is, to lowest order, the condition for the fixed point of Eq. (3) to be unstable (Sec. V). Substituting the results for  $E^{(0)}$  and  $F_2^{(1)}$  into the  $E^{(1)}$  equation and suppressing secularity so that it is possible to have  $E \approx E_c \exp(i\Delta\tau) + ik/\Delta$ , we get

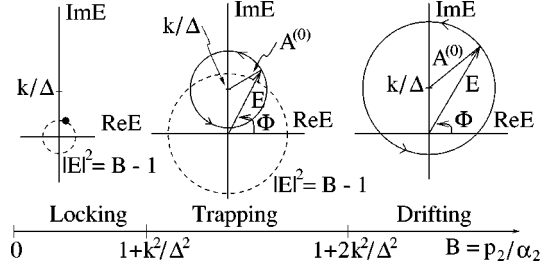


FIG. 2. The dependence of the behaviors of the phase difference  $\Phi$  on  $B$ , for  $k \sim \Delta = O(\sigma^a)$ ,  $a < 1/2$ . Parameters, variables, and symbols are as defined in Fig. 1.  $\Phi$  is constant if  $B < B_c$ , oscillates between  $\pi/2 \pm \tan^{-1}(\Delta A^{(0)}/k)$  if  $B_c < B < 1 + 2k^2/\Delta^2$ , and increases strictly if  $B > 1 + 2k^2/\Delta^2$ .  $A^{(0)}$  is as defined in Eq. (22). A supercritical Hopf bifurcation occurs at  $B = B_c$ . The bifurcation value for  $B$  has  $O(\sigma^{2-2a})$  errors [Eq. (16)] and the value of  $X_2$  has  $O(\sigma^{1-2a})$  errors [Eq. (26)]. Contrast this with Fig. 1, where phase trapping is impossible.

$$f = 0, \quad \theta^{(0)} = \frac{k^2}{\Delta^3} T + \psi^{(0)} = \sigma \frac{k^2}{\Delta^3} \tau + \psi^{(0)}$$

for some constant  $\psi^{(0)}$ . Hence, for time  $\tau = O(1/\sigma)$ , and assuming the system is *already on the attractor*, we find

$$E = A^{(0)} \exp \left\{ i \left[ \left( \Delta + \sigma \frac{k^2}{\Delta^3} \right) \tau + \psi^{(0)} \right] \right\} + \frac{ik}{\Delta} + O(\sigma) \quad (23)$$

$$F_2 = 1 + 2\sigma \frac{k}{\Delta^2} A^{(0)} \cos \left[ \left( \Delta + \sigma \frac{k^2}{\Delta^3} \right) \tau + \psi^{(0)} \right] + O(\sigma^2),$$

where  $A^{(0)} = \sqrt{B - B_c}$  and  $\psi^{(0)}$  is an arbitrary phase constant. These results have been compared with numerics and show good agreement. Note that the result is singular if  $\Delta \rightarrow 0$ . A similar singular limit has been observed in a model of a CO<sub>2</sub> laser [25].

## B. Discussion

### 1. Physical interpretation

An inspection of  $E$  in Eq. (23) reveals the following. (i) If  $A^{(0)} < k/\Delta$ , the phase difference  $\Phi$  oscillates between  $\pi/2 \pm \tan^{-1}(\Delta A^{(0)}/k)$ . The response laser is said to be *phase-trapped* to the drive [26]: both lasers have *the same average frequencies* but their relative phase varies periodically. In other words, they are frequency locked but not phase locked. (ii) If  $A^{(0)} > k/\Delta$ , then  $\Phi$  increases monotonically at an almost uniform rate, corresponding to a state of phase drift.

These different behaviors, together with the regimes in parameter space in which they occur, are depicted in Fig. 2. This figure should be compared with Fig. 1, which shows that for  $k = O(\Delta) \ll \sigma^{1/2}$ ,  $\Phi$  changes directly from locking to drifting at the critical pump value  $B = B_c + (\sigma^{2a})$ , with no intervening possibility of phase trapping.

Figure 3 illustrates the accuracy of our analytical approximations. For a given value of  $k$ , we compute the time series of the intensity  $I = X_2^2$ . The local minima and maxima of the intensity are plotted in Fig. 3 as a function of  $k$ . For  $k > 2$ , the intensity is constant because the system has a stable fixed point corresponding to a locked state; hence only a single-

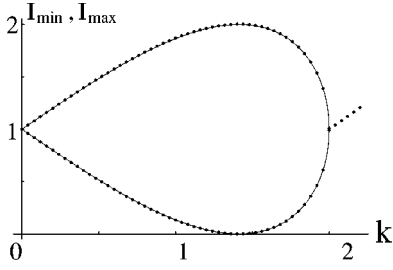


FIG. 3. Orbit diagram, plotting the local minima and maxima of the intensity  $I = X_2^2$  vs  $k$ , of Eq. (3), with  $\sigma = 0.010$ ,  $\Delta = 2.0$ ,  $k \in [0, 2.2]$ ,  $B = 2.0$ . Dots represent numerical results and curves theoretical expectations [Eq. (23)]. In this and subsequent orbit diagrams (Figs. 4 and 6), the numerical results are obtained by following the equation of motion with the subroutine STIFF in [W. H. Press, S. A. Teukolsky, W. T. Vetterling, and B. P. Flannery, *Numerical Recipes in Fortran: The Art of Scientific Computing*, 2nd ed. (Cambridge University Press, New York, 1992)], which implements a fourth-order Rosenbrock method, and then estimating the extremal values of the intensity with a second-order interpolation. The results are corroborated by another subroutine, STIFBS (*ibid*), which implements a semi-implicit extrapolation algorithm analogous to the Bulirsch-Stoer method.

valued branch of data is seen. As  $k$  decreases through the unlocking threshold, a limit cycle is born, causing two branches to bifurcate continuously from of the locked state, as shown in Fig. 3. This splitting is what one would expect for a supercritical Hopf bifurcation—the intensity now oscillates sinusoidally, so the lower branch corresponds to local minima of the intensity time series, and the upper branch corresponds to maxima. The curves passing through the data are analytical predictions given by Eq. (23).

While the solution (23) is periodic in the reference frame rotating with the driver, back in the laboratory frame the solution involves two frequencies. The phase of the receiver laser is then

$$\Phi_2 = \Phi_1 + \Phi \sim \Phi_{10} + \frac{\omega_1 \tau_{c,2}}{\alpha_2} \tau + \arg E$$

and is in general quasiperiodic.

## 2. Hopf bifurcation at $B = B_c + O(\sigma^2)$

The calculations in Sec. VII A, and in particular Eq. (22), are correct only to the lowest order in  $\sigma$ . If we proceed to higher orders, we find

$$A = \sqrt{B - \left( B_c + \frac{\sigma^2 B_c^2 (B_c - 1)}{\Delta^2} \right)} + O(\sigma^3).$$

From this and Eq. (23) we see that the radius of the stable limit cycle scales as  $\sqrt{B - B_{\text{bifn}}}$ , where  $B_{\text{bifn}} = B_c + O(\sigma^2)$  is the bifurcation value at which the limit cycle is born [compare with Eq. (16)], and the frequency  $\Delta + \sigma k^2 / \Delta^3$  is an  $O(1)$  quantity. These results strongly hint that this is a supercritical Hopf bifurcation [6]. Indeed, we can prove that this is the case for  $\sigma \ll 1$  and  $k, \Delta = O(1)$ , as follows.

For  $B$  close to  $B_{\text{bifn}}$ , we may take  $\varepsilon = B - B_{\text{bifn}}$  as a small parameter. By perturbing first with respect to  $\sigma$  and then with respect to  $\varepsilon$ , we find that the three eigenvalues at the relevant fixed point are

$$\lambda_1 = i \left( \Delta + \frac{\sigma k^2}{\Delta^3} \right) + \varepsilon \left[ \frac{1}{B_c} - \frac{\sigma k^2}{\Delta^4 B_c} (1 - i\Delta) \right] + O(\sigma^2, \varepsilon^2),$$

$$\lambda_2 = \overline{\lambda_1},$$

$$\lambda_3 = -\sigma B_c + \frac{2\varepsilon \sigma k^2}{\Delta^4 B_c} + O(\sigma^2, \varepsilon^2),$$

where an overbar denotes a complex conjugate. As  $\varepsilon$  goes through zero,  $\lambda_1$  and  $\lambda_2$  cross the imaginary axis with non-zero speed, while  $\lambda_3$  remains real and negative. Thus, by Hopf's theorem [27], a limit cycle is present on one side of the bifurcation point. Moreover, this limit cycle is centered at the fixed point, and has angular frequency given by the imaginary part of the conjugate pair of the eigenvalues. All these results are in agreement with Eq. (23), and we have also confirmed them numerically.

To decide whether the bifurcation is subcritical or supercritical, we use the Poincaré-Lindstedt method [6] to seek a periodic solution. We find that such a solution, be it stable or not, can exist only if  $B > B_{\text{bifn}}$ , i.e., when the fixed point is unstable, indicating that the bifurcation is supercritical. The periodic solution thus obtained is, as expected, the same as that given by Eq. (23). However, while the Poincaré-Lindstedt method tells us nothing about the stability of the solution, it has the merit that it is uniformly valid for all time, thus confirming the speculation, based on numerics and the two-timing analysis in Sec. VII A, that there is indeed a periodic solution.

## C. Rescaling for $\sigma \ll 1$ with $k = O(\Delta) \gg \sigma^{1/2}$

Having considered the case  $k, \Delta = O(1)$ , we will now demonstrate that as long as  $k = O(\Delta) \gg O(\sigma^{1/2})$ , the lowest-order dynamics remain the same as before. Thus, any coupling and detuning that satisfy these milder bounds are still sufficiently strong to preserve the qualitative features seen earlier. In this sense, the condition  $k = O(\Delta) \gg O(\sigma^{1/2})$  establishes the demarcation line for the regime of “strong” coupling and detuning.

By defining  $u$  via  $F_2 = 1 + \sigma u$ , we may rewrite Eq. (3) as

$$\frac{dX_2}{d\tau} = \sigma u X_2 + k \cos \Phi, \quad (24a)$$

$$\frac{d\Phi}{d\tau} = \Delta - \frac{k}{X_2} \sin \Phi, \quad (24b)$$

$$\frac{du}{d\tau} = B - (1 + \sigma u)(1 + X_2^2). \quad (24c)$$

For  $\Delta, k = O(1)$ , we observe in numerics that  $F_2 = 1 + O(\sigma)$  so that  $u = O(1)$ . More generally, if  $k, \Delta = O(\sigma^a)$ , we may write  $\Delta = \delta \sigma^a, k = \kappa \sigma^a$ , with  $\delta, \kappa = O(1)$ , and rescale time by setting  $t = \sigma^a \tau$ . Then Eq. (24) becomes

$$\frac{dX_2}{dt} = \sigma^{1-2a} u X_2 + \kappa \cos \Phi, \quad (25a)$$

$$\frac{d\Phi}{dt} = \delta - \frac{\kappa}{X_2} \sin \Phi, \quad (25b)$$

$$\frac{du}{dt} = B - (1 + \sigma^{1-a} u)(1 + X_2^2). \quad (25c)$$

For  $a < 1/2$ , our numerical simulations indicate that  $F_2 = 1 + O(\sigma^{1-a})$  so that  $u = O(1)$ . Hence we can invoke a self-consistent argument to identify, to lowest orders, Eq. (25) with Eq. (24), with  $\sigma^{1-2a}t, \delta, \kappa$  replacing  $\sigma, \tau, \Delta, k$ , respectively, since the terms  $\sigma u$  in Eq. (24c) and  $\sigma^{1-a}u$  in Eq. (25c) do not affect the lowest-order phenomena and are therefore negligible. As  $\delta, \kappa = O(1)$ , we can apply the same two-timing analysis as in Sec. VII A, but with the time scales  $t$  and  $\sigma^{1-2a}t$ , and get results similar to those found earlier. In terms of the variables used before rescaling, the lowest-order terms are found to be

$$\begin{aligned} X_2 e^{i\Phi} &= E = A^{(0)} \exp \left\{ i \left[ \left( \Delta + \sigma \frac{k^2}{\Delta^3} \right) \tau + \psi^{(0)} \right] \right\} + \frac{ik}{\Delta} \\ &\quad + O(\sigma^{1-2a}), \\ F_2 &= 1 + 2\sigma \frac{k}{\Delta^2} A^{(0)} \cos \left[ \left( \Delta + \sigma \frac{k^2}{\Delta^3} \right) \tau + \psi^{(0)} \right] \\ &\quad + O(\sigma^{2-2a, 3-5a}), \end{aligned} \quad (26)$$

where, as before,  $A^{(0)} = \sqrt{B - B_c} = \sqrt{B - 1 - k^2/\Delta^2}$  and  $\psi^{(0)}$  is an arbitrary phase constant. This result is the same as Eq. (23) to lowest order, exhibiting periodic motion born out of a supercritical Hopf bifurcation as  $B$  increases through  $B_c$  from below. One slight difference is that the next higher-order terms will be  $O(\sigma^{1-2a})$  instead of  $O(\sigma)$ . Also, corresponding behaviors in this new system will occur on a slower time scale, as  $t = \sigma^a \tau \ll \tau$ , if  $a > 0$ .

Clearly the argument above breaks down if  $a = 1/2$ , i.e., if  $k = O(\Delta) = O(\sigma^{1/2})$ , as then  $\sigma^{1-2a}$  in Eq. (25a) is no longer small as assumed by the perturbative treatment. Another way of putting this is that the two time scales, which are  $O(1)$  and  $O(\sigma^{-1+2a})$  in  $t$ , collapse into one as  $a \rightarrow 1/2$ . In the next section, we turn our attention to this distinguished regime  $k = O(\Delta) = O(\sigma^{1/2})$ . For symmetrically coupled lasers, this is the regime where subharmonic resonance, amplitude instabilities, and chaos were discovered [13,14].

## VIII. INTERMEDIATE COUPLING

### A. Overview

The cases studied earlier allow us to anticipate some aspects of the possible unlocking behavior for intermediate coupling. From Secs. V, VI, and VII, we know that for weak coupling ( $a > 1/2$ ), the fixed point corresponding to the stable locked state disappears in a saddle-node infinite-period bifurcation when  $B - B_c = O(\sigma^{2a})$ , while for strong coupling ( $a < 1/2$ ), it loses stability in a supercritical Hopf bifurcation when  $B - B_c = O(\sigma^{2-2a})$ . Hence, by sandwiching, we expect that for intermediate coupling ( $a = 1/2$ ), the stable fixed

point will lose stability when  $B - B_c = O(\sigma)$ , probably in a codimension-two bifurcation combining the features of a saddle-node infinite-period bifurcation and a supercritical Hopf bifurcation.

For  $B$  slightly above the bifurcation value, we expect the dynamics to be a combination of the two cases studied previously. The long-time behavior should be a spiraling motion that slowly passes through the bottleneck near

$$X_2 = \sqrt{B-1}, \quad \Phi = \sin^{-1} \left( \frac{\Delta \sqrt{B-1}}{k} \right), \quad F_2 = 1,$$

together with a fast reinjection roughly along the circle

$$X_2 = \sqrt{B-1}, \quad F_2 = 1.$$

Meanwhile, there is a global relaxation towards this attractor. The interplay among these three mechanisms can lead to complicated behavior, as we will see below.

In contrast, in the case of symmetrical coupling [ $\mu = 1$  in Eq. (2)], the phase difference decouples from the intensity and the gain, if one also assumes that both lasers have equal gains and intensities at all times [13]. This decoupling of the phase dynamics leaves only two mechanisms: a global relaxation toward the attractor, and a phase advancement (reinjection) along the attractor. In this sense, the unidirectionally coupled case might be prone to greater dynamical complexity.

### B. Numerics

In the intermediate coupling regime  $k = O(\Delta) = O(\sigma^{1/2})$ , Eq. (25) becomes

$$\frac{dX_2}{dt} = u X_2 + \kappa \cos \Phi,$$

$$\frac{d\Phi}{dt} = \delta - \frac{\kappa}{X_2} \sin \Phi,$$

$$\frac{du}{dt} = B - (1 + \sigma^{1/2} u)(1 + X_2^2), \quad (27)$$

with  $\kappa \sim \delta = O(1) \gg \sigma^{1/2}$ . In rectangular coordinates, with  $x = X_2 \cos \Phi, y = X_2 \sin \Phi$ , this system can be rewritten as

$$\frac{dx}{dt} = ux - \delta y + \kappa,$$

$$\frac{dy}{dt} = uy + \delta x, \quad (28)$$

$$\frac{du}{dt} = B - (1 + \sigma^{1/2} u)(1 + x^2 + y^2).$$

To probe the dynamics, we will vary  $\kappa$  and hold the other parameters fixed. This may seem unnatural, given that we have been using  $B$  as a control parameter so far. However, it turns out that if we vary  $\kappa$  instead of  $B$ , the features we wish to emphasize will stand out more clearly. In experiments, both parameters are easily tunable.

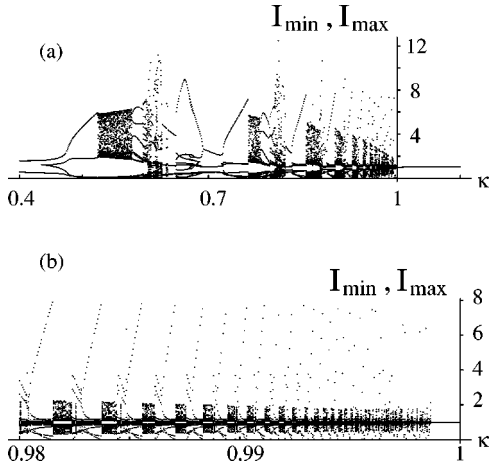


FIG. 4. Numerically computed orbit diagram of Eq. (27), with  $\sigma=0.0025$ ,  $\delta=1.0$ ,  $B=2.0$ . (a)  $\kappa \in [0.40, 1.1]$ ; (b) an enlargement in the range  $\kappa \in [0.98, 1.0]$ . Contrast the complicated patterns with the simple structure in Fig. 3. Note, in particular, the self-similar bifurcation sequence that piles up at  $\kappa=0.9986=\delta\sqrt{B-1}+O(\sigma)$ .

Figure 4 illustrates the complicated dynamics that occur in this system. The plot is an orbit diagram, shown in the same format as Fig. 3. The local minima and maxima of the intensity's time series are shown as the coupling  $\kappa$  increases toward the locking threshold. For the particular parameters chosen in the simulation, the locking threshold is at  $\kappa_c=0.9986=\delta\sqrt{B-1}+O(\sigma)$ . Of course, for  $\kappa>\kappa_c$ , the results are simple: there is a single branch of constant intensity, corresponding to the locked state. But for  $\kappa<\kappa_c$  we see an intricate pattern of local maxima and minima.

The most striking feature occurs for  $0.83 \leq \kappa \leq \kappa_c$ , where the diagram consists of a sequence of similar patterns that are scaled down as  $\kappa$  increases. Figure 4(b) shows the region close to  $\kappa=\kappa_c$  in greater detail. The self-similar structure appears to persist all the way to the unlocking threshold at  $\kappa=\kappa_c$ . This scenario is not the standard period-doubling route to chaos, nor any of the other familiar bifurcation cascades. We do not fully understand what is happening here. Some first steps toward understanding this remarkable structure will be presented in Sec. IX.

We are mainly interested in the self-similar structure near the unlocking threshold, but some other features of Fig. 4 deserve comment. An unsuspecting look at Fig. 4(a) might suggest that the attractor is quasiperiodic or chaotic for  $0.52 \leq \kappa \leq 0.58$ , as we see a complex set of data there. But this conclusion is premature, as a highly looped periodic attractor with many turning points could also generate such a picture, thanks to the many local minima and maxima in its corresponding time series.

Figure 5 shows that, in fact, this is exactly what is happening for many values of  $\kappa$  in the range  $0.52 \leq \kappa \leq 0.58$ . The  $xy$  projections of the attractors in phase space are plotted using DSTOOL [28]. The orbit in Fig. 5(a) appears to be quasiperiodic, while those in Figs. 5(b)–5(e) appear periodic. These figures also suggest that several kinds of bifurcations are taking place. The trio Figs. 5(c)–5(e) indicates a period-doubling sequence, although we do not see the full period-doubling cascade to chaos.

Hence, to distinguish whether the long-term behavior is

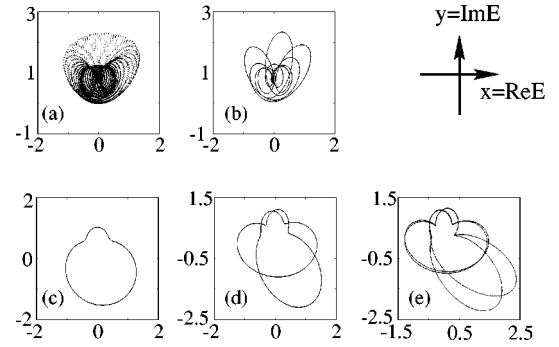


FIG. 5. The  $xy$  projections of the attractors of Eq. (27), with  $\sigma=0.0025$ ,  $\delta=1.0$ ,  $B=2.0$ . (a)  $\kappa=0.78$ , a quasiperiodic attractor. We have followed the flow only for a time span of 1000 units in order to reveal the structure. (b)  $\kappa=0.77$ , a periodic attractor with many local minima and maxima. This attractor remains a closed curve without blurring in a time span of 2000 units, strongly hinting at its periodicity. (c)  $\kappa=0.70$ , a period-1 orbit. (d)  $\kappa=0.68$ , a period-2 orbit. (e)  $\kappa=0.67$ , a period-4 orbit.

periodic or not for a given set of parameters, a more careful treatment, such as plotting the power spectrum, is needed. We have computed the largest Lyapunov exponent as a function of  $\kappa$ , with other parameters fixed, and find that it is always zero, up to the accuracy of the numerical algorithms. This result suggests that there is probably no chaos in the intermediate coupling regime considered here. Perhaps a more prudent way to put it is this: chaos is not widespread for intermediate coupling, if it occurs at all.

There are many other interesting attractors and bifurcations that could be discussed here, but we prefer to skip them so that we can focus our attention on the self-similar picture near the unlocking threshold.

## IX. A SINGULAR LIMIT

We now consider a simpler system that exhibits the same cascade found in Fig. 4. Let  $\sigma=0$  in the reduced system (27), so that it becomes

$$\begin{aligned} \frac{dX_2}{dt} &= uX_2 + \kappa \cos \Phi, \\ \frac{d\Phi}{dt} &= \delta - \frac{\kappa}{X_2} \sin \Phi, \\ \frac{du}{dt} &= B - (1 + X_2^2). \end{aligned} \quad (29)$$

Figure 6 shows that this new system still exhibits the striking pattern found earlier (although the precise positions of the bifurcations are not the same, and there are structures that come up in one case but not the other). This robustness suggests that the self-similar cascade is not due to perturbative effects of  $\sigma$  but is more generic. To check that the cascade is not just an artifact of the choice of variables plotted, we have also tried plotting local minima and maxima of  $x, y, u$ , and  $I=x^2+y^2$  against the parameter  $\kappa$ . In all cases, we find similar patterns. We have also checked that the patterns keep recurring even closer to the unlocking threshold, specifically for  $\kappa \in [0.998, 1]$  and  $\kappa \in [0.9998, 1]$ . So we believe that the self-similarity is genuine.

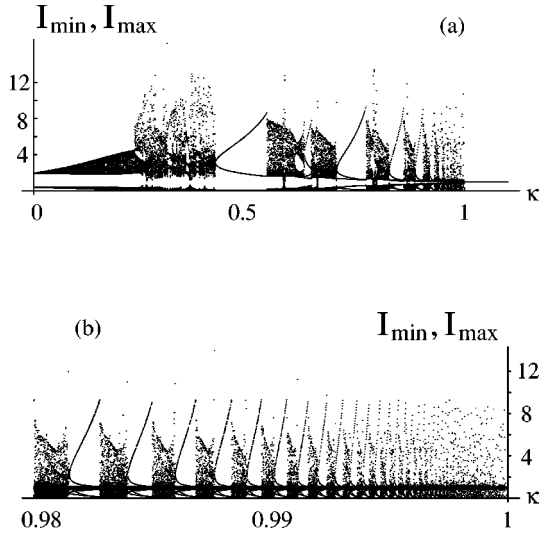


FIG. 6. Numerically computed orbit diagram of Eq. (29), with  $\delta=1.0$ ,  $B=2.0$ . (a)  $\kappa \in [0, 1.1]$ ; (b)  $\kappa \in [0.98, 1.0]$ . Compare with Fig. 4.

On the other hand, the limit  $\sigma=0$  requires some caution on our part. The blown-up system (27) is obtained from Eq. (3) by the rescaling  $t=\sigma^{1/2}\tau$ ,  $\sigma^{1/2}u=F_2-1$ ,  $\Delta=\sigma^{1/2}\delta$ ,  $k=\sigma^{1/2}\kappa$ , which becomes *singular* as  $\sigma \rightarrow 0$ . Hence Eq. (29) is not directly relevant physically, but it has the virtue that it leads to cleaner numerics, and brings out the bifurcation mechanism more clearly.

One should also be aware that the singular limit displays some nongeneric dynamics because of its higher degree of symmetry than the original system. For instance, Eq. (29) is invariant under the transformation

$$\mathcal{T}: t \rightarrow -t, \quad x \rightarrow -x, \quad y \rightarrow y, \quad u \rightarrow -u, \quad (30)$$

a ‘‘reversibility’’ symmetry that is not preserved by Eq. (27) for  $\sigma \neq 0$ . A corollary of this invariance is that if  $\Omega$  is an attractor, then the set  $\tilde{\Omega} = \{(x, y, u) | (-x, y, -u) \in \Omega\}$  is a repeller. Results like this can be used for checking numerical convergence in tracing bifurcation diagrams.

### A. Fixed-point analysis

Since the transformation from Eq. (3) to Eq. (29) is singular, the fixed-point analysis (both existence and stability) in Sec. V is not directly applicable to Eq. (29). The necessary modification is straightforward, and the result is as follows. Fixed points exist if and only if  $1 \leq B \leq B_c \equiv 1 + \kappa^2/\delta^2$ . They are given by  $p_{\pm} = (\pm x^*, y^*, \pm u^*)$ , where

$$x^* = \frac{\delta}{\kappa} \sqrt{(B-1)(B_c-B)},$$

$$y^* = \frac{\delta}{\kappa} (B-1),$$

$$u^* = -\delta \sqrt{\frac{B_c-B}{B-1}}.$$

Hence both fixed points recede to infinity as  $B \rightarrow 1^+$ , and they coalesce at  $(0, \kappa/\delta, 0)$  as  $B \rightarrow B_c^-$ .

As for stability, the Jacobian of Eq. (29) is

$$J = \begin{bmatrix} u & -\delta & x \\ \delta & u & y \\ -2x & -2y & 0 \end{bmatrix}.$$

At the fixed points, the characteristic equation simplifies to

$$0 = f_u(\lambda) \equiv \lambda^3 - 2u\lambda^2 + \frac{\kappa^2}{B-1}\lambda + 2(B-1)(\lambda - u), \quad (31)$$

where  $u = u_{\pm}^*$  at the fixed point  $p_{\pm}$ . Since  $f_{-u}(-\lambda) = -f_u(\lambda)$  and  $u_+^* = -u_-^*$ , we can conclude that if  $\lambda$  is an eigenvalue of  $p_+$ , then  $-\lambda$  is an eigenvalue of  $p_-$ . Hence we cannot have a saddle-node bifurcation at  $B = B_c$ .

The eigenvalue equation (31), as it stands, is hard to solve. But some information can be obtained from the intermediate value theorem. Since  $f_u(\pm\infty) = \pm\infty$ , and  $f_{u_{\pm}^*}(0) = \pm 2(B-1)\delta\sqrt{(B_c-B)/(B-1)}$  is positive (negative) at  $p_+$  ( $p_-$ ), the intermediate value theorem implies that the fixed point  $p_-$  always has a positive eigenvalue and therefore cannot be stable. Whether it is a saddle or a repeller is not determined by this argument.

To investigate the type of bifurcation at  $B = B_c$ , we will consider Eq. (31) with  $B = B_c - \varepsilon$ , where  $\varepsilon > 0$  is a small parameter, and  $\kappa$  and  $\delta$  are assumed to be  $O(1)$  positive quantities. Then we have a regular perturbation problem and can find the eigenvalues to be

$$\lambda_{1,2} = \pm i \sqrt{\delta^2 + 2\kappa^2/\delta^2} - \frac{\delta^6 + \kappa^2\delta^2}{\kappa\delta^4 + 2\kappa^3} \sqrt{\varepsilon} + O(\varepsilon), \quad (32)$$

$$\lambda_3 = \frac{-2\kappa\delta^2}{\delta^4 + 2\kappa^2} \sqrt{\varepsilon} + O(\varepsilon)$$

at  $p_+$ . Hence  $p_+$  is an attractor. More specifically, it is an attracting ‘‘spiral node.’’ The eigenvalues at  $p_-$  can be obtained by taking the negatives of the eigenvalues of  $p_+$ .

These results provide some local information about the bifurcation at  $B = B_c$ . As  $B \rightarrow B_c^-$ , i.e.,  $\varepsilon \rightarrow 0^+$ , the two fixed points approach each other and collide at  $B = B_c$ . Meanwhile, their attractiveness and repulsiveness get weaker and weaker, since *all* the eigenvalues approach the imaginary axis. The fixed point at  $B = B_c$  is linearly neutrally stable.

As Eq. (32) indicates, locally the bifurcation is of codimension two, with a simple zero eigenvalue and a conjugate pair of pure imaginary eigenvalues. As noted in [18], such bifurcations can be complex because of their global structures. In Eq. (29), as in Eq. (24), the reinjection provides such a global mechanism that leads to complicated dynamics.

Since the stable fixed point is annihilated in a collision with an unstable object as  $B \rightarrow B_c^-$ , we do not expect stable objects for  $B > B_c$  to be in small neighborhoods of  $(0, \delta(B_c - 1)/\kappa, 0)$ , the position of the fixed point at  $B = B_c$ . However, some form of intermittency might be expected, and as we show in the next section, this is indeed the case. A tra-

jectory on the periodic attractors spends a long time in helical motion near the ghost of the fixed point. The same is true when  $\sigma > 0$ , indicating that this helical motion in the bottleneck is not caused by the degeneracy.

Before we move on to numerics, it should be noted that this degenerate ‘‘attractor-repellor bifurcation’’ is a consequence of setting  $\sigma$  to zero. For  $\sigma > 0$ , a generic saddle-node bifurcation occurs at  $B = B_c$ . Also, for  $\sigma > 0$ , generically we do not have a genuine codimension-two bifurcation. But since both  $H_1$  and  $H_3$  in condition (12) vanish at  $B_c + O(\sigma)$ , meaning that all three eigenvalues are close to the imaginary axis when bifurcation occurs, the nonsingular system (27) may pick up some remnants of the bifurcation scenario of the singular system (29), so that their orbit diagrams (Figs. 4 and 6) exhibit similar features. This suggests that whatever the bifurcation scenario is, it is stable with respect to perturbations in parameters, at least in an operational sense.

### B. Numerical studies of the self-similar bifurcation sequence

In our numerical studies of the self-similar bifurcation sequence, we concentrate on the periodic windows. As before, we will vary  $\kappa$  and keep other parameters fixed. Then for  $\kappa = \kappa_c + \varepsilon$ , with  $0 \leq \varepsilon \ll 1$  and  $\kappa_c \equiv \delta\sqrt{B-1}$ , the fixed points are at  $p_{\pm} = (\pm x^*, y^*, \pm u^*)$ , where

$$\begin{aligned} x^* &= \frac{1}{\delta} \sqrt{2\varepsilon\kappa_c} \left( 1 - \frac{3\varepsilon}{4\kappa_c} \right) + O(\varepsilon^{5/2}), \\ y^* &= \frac{\kappa_c}{\delta} \left( 1 - \frac{\varepsilon}{\kappa_c} \right) + O(\varepsilon^2), \\ u^* &= -\frac{\delta}{\kappa_c} \sqrt{2\varepsilon\kappa_c} \left( + \frac{\varepsilon}{4\kappa_c} \right) + O(\varepsilon^{5/2}). \end{aligned}$$

The eigenvalues at  $p_+$  are

$$\begin{aligned} \lambda_{1,2} &= \pm i \sqrt{\delta^2 + 2\kappa_c^2/\delta^2} - \delta \sqrt{\frac{2}{\kappa_c} \frac{\delta^4 + \kappa_c^2}{\delta^4 + 2\kappa_c^2}} \sqrt{\varepsilon} + O(\varepsilon), \\ \lambda_3 &= \frac{-\delta(2\kappa_c)^{3/2}}{\delta^4 + 2\kappa_c^2} \sqrt{\varepsilon} + O(\varepsilon). \end{aligned} \quad (33)$$

#### 1. Helical structure of the periodic attractors

Using AUTO, we have examined the phase-space geometry of the attractors in individual periodic windows. For definiteness, consider the  $yu$  projections of the attractors. Figure 7 shows a typical collection of snapshots as we sweep  $\kappa$  across a window. What happens in this window also happens in other windows, with some modifications in details. Specifically, we see  $n$  little helical loops per round trip at the left end of the  $n$ th window. (In this example,  $n = 7$ .) Most of these loops are located near  $(0, 1, 0)$ , where the stable fixed point is annihilated at  $\kappa = 1$ .

Intuitively, the trajectory is slowly funneled through the bottleneck caused by the ghost of the former stable fixed point. During this slow passage, the trajectory also spirals around at an  $O(1)$  frequency, given by the imaginary part of

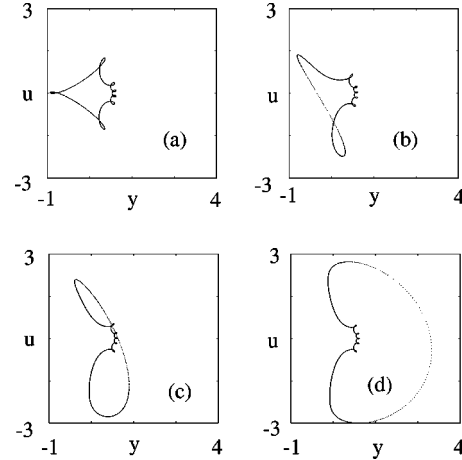


FIG. 7. The  $yu$  projections of the attractors of Eq. (29) as we sweep across the  $n = 7$  periodic window by increasing  $\kappa$ , with  $\delta = 1.0$ ,  $B = 2.0$ . (a)  $\kappa = 0.91867$ ; (b)  $\kappa = 0.92500$ ; (c)  $\kappa = 0.92980$ ; (d)  $\kappa = 0.93200$ . The snapshots are not taken at evenly spaced values of  $\kappa$ . Rather, representatives are chosen to show the deformations more clearly.

the complex eigenvalues in Eq. (33). The combination of slow passage and  $O(1)$  spiraling gives rise to the helical appearance of the trajectories.

As we increase  $\kappa$  in a periodic window,  $(n-2)$  of these loops stay at roughly the same distance from the  $u$  axis, while the remaining two loops are stretched in the reinjection part of the flow. Moreover, the left side of the projection moves, with a stronger shear at the bottom, towards the  $u$  axis, eventually crossing the loops. Meanwhile, there is a clockwise rotation to bring about the structure we see as we reach the right-hand end of the window. The same trend occurs in all the periodic windows we have sampled, with  $3 \leq n \leq 12$  (we do not see periodic windows corresponding to  $n = 1, 2$ ). If this ‘‘ $n$  loops in the  $n$ th window’’ scenario is correct, and if there really exist infinitely many such windows accumulating at the limiting value  $\kappa = 1$ , we will have an attractor with infinitely many tight loops at  $\kappa = 1^-$ , just before its annihilation in an attractor-repellor bifurcation. This will then be reminiscent of the chaotic orbit born from the infinite sequence of period doubling in the logistic map.

In a similar problem concerning a  $\text{CO}_2$  laser, Zimmermann, Natiello, and Solari [29] worked backwards and constructed a model by assembling a local spiral motion and a global reinjection. Numerically, for a fixed set of parameters, the flow is similar to what we see here. However, how this mathematical model is related to the original laser system is unclear.

#### 2. How periodicity ends

In each periodic window, the unstable branch always has its nontrivial Floquet multipliers outside the unit circle, indicating a repellor instead of a saddle. When this branch collides with the stable branch, an attractor-repellor bifurcation of cycles occurs, bringing an end to the periodic window. In virtue of the invariance of Eq. (29) under the transformation (30), it is no wonder that at the bifurcations, when the attractor and the repellor coalesce, this neutrally stable object is invariant under  $\mathcal{T}' : x \rightarrow -x, y \rightarrow y, u \rightarrow -u$ . This explains why the projections onto the  $yu$  plane are always sym-

metrical with respect to  $u \rightarrow -u$  [as seen in Figs. 7(a) and 7(d)], while the projections onto the  $xy$  plane are always symmetrical with respect to  $x \rightarrow -x$  at the ends of the windows (not shown).

As mentioned earlier, the attractor-repeller bifurcations are a consequence of the reversibility symmetry of the  $\sigma = 0$  system. Generically, the periodic attractors are annihilated in saddle-node bifurcations and there is no  $\mathcal{T}$  symmetry, a strong indication that the mechanism underlying the cascade of bifurcations has nothing to do with this symmetry.

Recalling the results in Sec. IX A, we notice that while an attractor-repeller bifurcation of fixed points occurs as the locking threshold is approached from above ( $\kappa \rightarrow 1^+$ ), there is a simultaneous attractor-repeller bifurcation of cycles (presumably with infinitely many loops) as the threshold is approached from below ( $\kappa \rightarrow 1^-$ ). This double-sided aspect of the unlocking bifurcation also seems to be preserved for  $\sigma > 0$ , suggesting that it too has nothing to do with symmetry.

### 3. Trends in the periodic windows

The periodic windows in Fig. 6 have been verified by AUTO to be isolas, i.e., they terminate at both ends as the periodic attractors are annihilated in collisions with unstable objects (probably unstable periodic orbits). However, we do not fully understand the mechanism that causes such annihilations, although it seems to be some form of resonance of the spiraling motion and the global reinjection. Indeed, we have found that as we increase  $\kappa$  in a periodic window, periodicity ends precisely when a trajectory executes an integer number of spiral loops upon one reinjection, i.e., if

$$\frac{2\pi}{\omega_I} = n \frac{2\pi}{\omega_S}, \quad (34)$$

where  $n$  is a positive integer, and  $\omega_I$  and  $\omega_S$  are the frequencies of the reinjection and the spiraling motion, respectively. To see this, we assume that the time needed for reinjection is dominated by the slow passage through the bottleneck. Then, using Eq. (33), we may rewrite Eq. (34) as

$$\frac{\delta(2\kappa_c)^{3/2}}{\delta^4 + 2\kappa_c^2} \sqrt{\varepsilon_n} = \frac{1}{n} \sqrt{\delta^2 + 2\kappa_c^2/\delta^2}$$

to lowest order, where  $\varepsilon_n = 1 - \kappa_{R,n}$ , and  $\kappa_{R,n}$  is where the  $n$ th periodic window ends at the right. Solving for  $\varepsilon_n$ , we get

$$\varepsilon_n = \frac{(\delta^4 + 2\kappa_c^2)^3}{\delta^4(2\kappa_c)^3} \frac{1}{n^2}. \quad (35)$$

Moreover, at these parameter values, corresponding to the right ends of the periodic windows, the periods of the attractors are expected to be

$$T_{R,n} \approx \frac{2\pi}{\omega_I} = 2\pi \frac{\delta^4 + 2\kappa_c^2}{\delta(2\kappa_c)^{3/2}} \frac{1}{\sqrt{\varepsilon_n}} = \frac{2\pi\delta}{\sqrt{\delta^4 + 2\kappa_c^2}} n. \quad (36)$$

Figures 8(a) and 8(b) compare these predicted scaling laws against numerics. For  $n \geq 5$ , Eqs. (35) and (36) agree with numerics to within 2%.

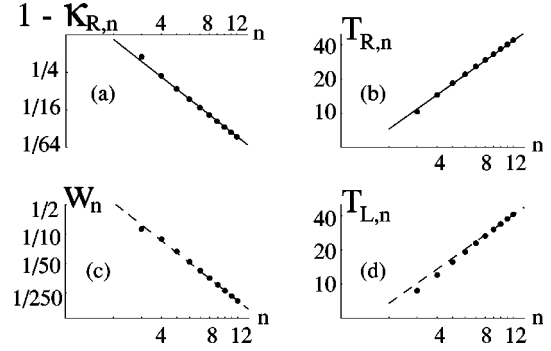


FIG. 8. Log-log plots showing the trends among the periodic windows of Eq. (29) with  $\delta = 1.0$ ,  $B = 2.0$ , in the (a) positions of the right ends of the periodic windows, with the theoretical prediction  $\ln(1 - \kappa_{R,n}) = \ln(27/8) - 2 \ln n$ ; (b) periods of the attractors at the right ends of the periodic windows, with the theoretical prediction  $\ln T_{R,n} = \ln(2\pi/\sqrt{3}) + \ln n$ ; (c) widths, with the fit  $\ln w_n = 1.5 - 3 \ln n$ ; and (d) periods of the attractors at the left ends of the periodic windows, with the fit  $\ln T_{L,n} = 1.2 + \ln n$ . Dots represent raw data with  $3 \leq n \leq 12$ , solid lines represent theoretical predictions [Eqs. (35) and (36)] with no fitting parameter, and dashed lines represent semitheoretical predictions, where the slopes are chosen according to the theoretical scaling [Eqs. (37) and (38)], and the intercepts are chosen to fit the data.

We do not know what mechanism kills the periodic window as we decrease  $\kappa$ . But drawing an analogy to the mechanism at the other end, we expect that the positions of the left ends of the periodic windows scale as

$$1 - \kappa_{L,n} = O(1/n^2),$$

so that the widths of the periodic windows scale as

$$w_n = \kappa_{R,n} - \kappa_{L,n} = O(1/n^3), \quad (37)$$

and the periods of the attractors at the left ends of the periodic windows scale as

$$T_{L,n} = O(n). \quad (38)$$

These scaling behaviors are verified in Figs. 8(c)–8(d).

Meanwhile, the sizes of the attractors, as measured by the  $L^2$  norms, remain  $O(1)$  as  $\kappa \rightarrow 1^-$ . This is expected as the  $L^2$  norm is dominated by the global reinjection, which persists in all periodic windows.

## X. OPEN QUESTIONS

From a theoretical perspective, the most interesting open question concerns the mathematical mechanism underlying the self-similar cascade of bifurcations observed in both Eq. (27) and the simpler system (29). Whatever the mechanism is, the heuristic arguments and numerical evidence presented in Sec. IX suggest that it must combine the features of a saddle-node infinite-period bifurcation and a supercritical Hopf bifurcation. As such, it may well arise in other scientific settings. Maybe it can even be detected experimentally.

Although self-similarity itself is common in dynamical systems, and has been explained by renormalization-group arguments in such contexts as period doubling, intermittency, and quasiperiodic breakdown [18], it seems the cas-

cade we see here falls into none of these categories. Rather, it is characterized by an infinite series of saddle-node bifurcations of cycles, accumulating at a finite parameter value corresponding to the locking threshold.

Aside from these bifurcation issues, the dynamics of Eq. (29) is also interesting for a *fixed* set of parameters. Zimmermann, Natiello, and Solari [29] suggested that the periodic orbits with many small loops can be understood as the effects of a flow with helical local dynamics together with a global reinjection. The challenge now is to find a way to reduce the laser equations to a form where this conjectured phase-space geometry becomes transparent.

There are many other interesting avenues for future research. The dynamics of the unidirectionally forced system could be explored over a much broader range of parameter values, with  $k$  and  $\Delta$  not necessarily of the same order. We have also neglected the effects of noise, a topic of great importance in technological applications of injection locking [11,30–32]. Another promising direction would be to study arrays of coupled lasers [33–39] driven by external injection, particularly in regimes where amplitude effects are important and the phase model approximation is not valid. Finally, we

have restricted attention to drive signals of constant intensity and frequency, but for applications to optical communications [40,41], one needs to study how lasers respond to modulated drive signals, especially those carrying messages within them.

#### ACKNOWLEDGMENTS

We thank John Guckenheimer for discussions on period doubling and the self-similar bifurcation sequence, Jim Keener for pointing out that essential singularities can give rise to self-similar bifurcation sequences, Rajarshi Roy and Scott Thornburg for discussions on the physical interpretation of our results and for references to the laser literature, and Paul Steen for commenting on an early draft of this paper and for providing technical advice regarding AUTO. We also thank Henry Abarbanel, Rajarshi Roy, and the other members of the UCSD–Georgia Tech–Cornell collaboration on synchronization and communication in nonlinear optical systems. The research was supported in part by the National Science Foundation.

- 
- [1] R. Adler, Proc. IRE **34**, 351 (1946), reprinted in Proc. IEEE **61**, 1380 (1973).
- [2] G. Grüner, Physica D **8**, 1 (1983).
- [3] G. B. Ermentrout and J. Rinzel, Am. J. Physiol. **246**, R102 (1984).
- [4] S. H. Strogatz, J. Math. Biol. **25**, 327 (1987).
- [5] W. C. Stewart, Appl. Phys. Lett. **12**, 277 (1968).
- [6] S. H. Strogatz, *Nonlinear Dynamics and Chaos: with Applications in Physics, Biology, Chemistry, and Engineering* (Addison-Wesley, Reading, MA, 1994).
- [7] (a) A. E. Siegman, *Lasers* (University Science Books, Mill Valley, CA, 1986), p. 1153; (b) p. 1148.
- [8] C. O. Weiss and R. Vilaseca, *Dynamics of Lasers* (VCH, New York, 1991).
- [9] C. J. Buczek, R. J. Freiberg, and M. L. Skolnick, Proc. IEEE **61**, 1411 (1973).
- [10] R. L. Byer, in *Solid State Lasers: New Developments and Applications*, Vol. 317 of *NATO Advanced Study Institute Series B: Physics*, edited by M. Inguscio and R. Wallenstein (Plenum, New York, 1993).
- [11] R. Barillet, Ann. Telecommun. **51**, 553 (1996).
- [12] T. Erneux, R. Kuske, and T. W. Carr, Proc. SPIE **2792**, 54 (1995).
- [13] K. S. Thornburg, Jr., M. Möller, R. Roy, T. W. Carr, R.-D. Li, and T. Erneux, Phys. Rev. E **55**, 3865 (1997).
- [14] T. Erneux, S. M. Baer, and P. Mandel, Phys. Rev. A **35**, 1165 (1987).
- [15] I. B. Schwartz and T. Erneux, SIAM (Soc. Ind. Appl. Math.) J. Appl. Math. **54**, 1083 (1994).
- [16] L. Fabiny, P. Colet, R. Roy, and D. Lenstra, Phys. Rev. A **47**, 4287 (1993).
- [17] Alternatively, we may use rectangular coordinates, with  $x = X_2 \cos \Phi$ ,  $y = X_2 \sin \Phi$  to avoid the notational difficulty regarding the case  $X_2 = 0$ . The results are of course the same.
- [18] J. Guckenheimer and P. Holmes, *Nonlinear Oscillations, Dynamical Systems and Bifurcations of Vector Fields* (Springer-Verlag, New York, 1985).
- [19] J. V. Uspensky, *Theory of Equations* (McGraw-Hill, New York, 1948), p. 304.
- [20] W. Hahn, *Stability of Motion* (Springer-Verlag, New York, 1967), p. 19.
- [21] At  $B = B_c = 1 + \kappa^2 / \delta^2$ , there are three, not two, fixed points. They are at  $1 + \kappa^2 / (2\delta^2) \pm \sqrt{\kappa^4 / (4\delta^4) - \sigma^{2a}\delta^2 - \sigma^{2a}\kappa^2}$  and 1. These are equivalent to  $B_c - \sigma^{2a}\kappa^2 B_c / (B_c - 1)^2 + O(\sigma^{4a})$ ,  $1 + \sigma^{2a}\kappa^2 B_c / (B_c - 1)^2 + O(\sigma^{4a})$ , and 1 (exact), in agreement with Eqs. (13) and (14). There is no collision of fixed points at  $B = B_c$ .
- [22] If we start from a set of parameters such that condition (12) holds and vary parameters continuously, we cannot have  $H_2 = 0$  or  $H_2' = 0$  without having one of the other two inequalities becoming an equality first. Hence we can concentrate on  $H_1$  and  $H_3$  when we look for bifurcation points.
- [23] D. Zwillinger, *Handbook of Differential Equations*, 2nd ed. (Academic Press, Boston, 1992).
- [24] E. J. Doedel, X. J. Wang, and T. F. Fairgrieve, *AUTO94: Software for Continuation and Bifurcation Problems in Ordinary Differential Equations* (Center for Research on Parallel Computing, California Institute of Technology, Pasadena, California, 1996).
- [25] H. G. Solari and G.-L. Oppo, Opt. Commun. **111**, 173 (1994).
- [26] R. E. Kronauer *et al.*, Am. J. Physiol. **242**, R3 (1982).
- [27] L. N. Howard and N. Kopell, in *The Hopf Bifurcation and Its Applications*, edited by J. E. Marsden and M. F. McCracken, Applied Mathematical Sciences (Springer-Verlag, New York, 1976), Vol. 19, Chap. 5.
- [28] J. Guckenheimer, M. R. Myers, F. J. Wicklin, and P. A. Worfolk, *DsTool: A Dynamical System Toolkit with an Interactive Graphical Interface* (Center for Applied Mathematics, Cornell University, Ithaca, New York, 1995).

- [29] M. G. Zimmermann, M. A. Natiello, and H. G. Solari, *Physica D* **109**, 293 (1997).
- [30] H.-A. Bachor *et al.*, *Proc. SPIE* **2799**, 157 (1995).
- [31] I. Freitag and H. Welling, *Appl. Phys. B: Lasers Opt.* **58**, 537 (1994).
- [32] A. D. Farinas, E. K. Gustafson, and R. L. Byer, *J. Opt. Soc. Am. B* **12**, 328 (1995).
- [33] Y. Braiman, T. A. B. Kennedy, K. Wiesenfeld, and A. I. Khibnik, *Phys. Rev. A* **52**, 1500 (1995).
- [34] A. I. Khibnik, Y. Braiman, T. A. B. Kennedy, and K. Wiesenfeld, *Physica D* **111**, 295 (1998).
- [35] M. Silber, L. Fabiny, and K. Wiesenfeld, *J. Opt. Soc. Am. B* **10**, 1121 (1993).
- [36] R.-D. Li and T. Erneux, *Phys. Rev. A* **46**, 4252 (1992).
- [37] R.-D. Li and T. Erneux, *Phys. Rev. A* **49**, 1301 (1994).
- [38] I. M. Bel'dyugin, M. V. Zolotarev, and I. V. Shinkareva, *Quantum Electron.* **27**, 35 (1997).
- [39] A. Hohl, A. Gavrielides, T. Erneux, and V. Kovanis, *Phys. Rev. Lett.* **78**, 4745 (1997).
- [40] P. Colet and R. Roy, *Opt. Lett.* **19**, 2056 (1994).
- [41] G. D. VanWiggeren and R. Roy, *Science* **279**, 1198 (1998).